Dual-Band Metamaterial Microwave Absorber using Ring and Circular Patch with Slits

Man Seng Sim[1], Kok Yeow You[1], Raimi Dewan[1], Fahmiruddin Esa[2], Mohd Rashidi Salim[1], Stephanie Yen Nee Kew[1], and Fandi Hamid[1]

[1]Faculty of Electrical Engineering, Universiti Teknologi Malaysia, 81310 Johor Bahru, Malaysia

[2]Faculty of Applied Sciences and Technology, Pagoh Higher Education Hub, Universiti Tun Hussein Onn Malaysia, 84600 Panchor, Malaysia

Corresponding author: Kok Yeow You (e-mail: kyyou@fke.utm.my).

ABSTRACT This paper proposes a dual-band metamaterial microwave absorber operating at 2.5 GHz and 5.8 GHz. The absorber consists of a ring and a circular patch with slits resonator structures printed on an FR4 dielectric substrate backed by a ground layer. The main advantage of the absorber lies in its design flexibility, where each absorption band is independent and can be individually tuned by changing the dimensions of each resonator structure. The absorber unit cell is simulated and parametrically optimized using Computer Simulation Technology (CST) software. The absorption mechanism is analyzed based on surface current analysis and symmetric model method. The absorber prototype, with dimensions of $200 \times 200 \times 1.6$ mm^3 and consisting of an array of 7×7 unit cells, is fabricated and experimentally investigated using antennas in free-space measurement. The absorber exhibits over 97% absorption at both resonance frequencies. Furthermore, the absorber is demonstrated to be applicable in sensing applications for dielectric constant determination. With its design simplicity, wide-angle receptive, and polarization insensitive behavior, it is envisaged that the proposed absorber will find practical use in absorbing and sensing applications.

INDEX TERMS Absorption, Dielectric constant, Metamaterial, Metasurface, Resonator, Sensor.

I. INTRODUCTION

METAMATERIAL microwave absorbers are periodically arranged unit cell structures which achieve near perfect absorption within a specific frequency range. The applications of absorbers include electromagnetic interference (EMI) shielding, radar cross-section (RCS) reduction, filters, energy harvesters, and sensors [1].

Numerous efforts have been carried out to design metamaterial with multiband absorption characteristics. One approach involves combining several resonators of different geometries, sizes, or rotational arrangements within a single unit cell. For instance, T-shaped resonators [2], meandered line resonators [3], and L-shaped resonators [4] are proposed to be arranged in a rotational manner within a same unit cell. Due to the mutual coupling effect between the resonators, their combined arrangement often results in a distinct absorption response compared to that of their constituent resonators. This leads to complexity in design work as the combined resonators work as a whole unified structure and individual tuning of each absorption peaks to designated frequency ranges becomes challenging. Another approach to achieving multiband absorption involves designing three-dimensional (3D) or multilayer structures [5]. However, this increases the overall size of the absorber and limits its

practical applications. Moreover, multilayer structures are susceptible to misalignment between layers, which could potentially compromise the absorber performances.

Some designs of metamaterial absorbers are sensitive to the angle of incidence and polarization [6]. Under oblique angles of incidence or polarization, the absorption may diminish or shift to other frequencies. Additionally, designing a multiband metamaterial absorber structure can be complex as they usually consist of intertwined resonators which lead to difficulty in tuning the absorption bands individually [7].

In this study, a dual-band microwave absorber operating simultaneously at 2.5 GHz and 5.8 GHz is proposed. The absorption is achieved by combining two resonators (an outer ring and an inner circular patch with slits) in a unit cell structure. The ring and the circular patch contribute to the absorption at 2.5 GHz and 5.8 GHz, respectively. Both structures are not intertwined and can be individually modified to a certain extent to operate at other frequency ranges. The article is organized as follows: Section II discusses the design, simulation, parametric optimization, fabrication, and experimental measurement processes of the metamaterial absorber. In Section III, the absorption performance and mechanism of the absorber are discussed, and its applications in dielectric material characterization are

demonstrated. Finally, conclusions are presented in Section IV.

II. METHODOLOGY

The operation principle of a metamaterial absorber is briefly explained as follows. The absorptivity, α of a planar metamaterial absorber is determined by [5]:

$$\alpha = 1 - |S_{11}|^2 - |S_{21}|^2 \tag{1}$$

where $|S_{11}|$ and $|S_{21}|$ are the linear magnitude of reflection coefficient and linear magnitude of transmission coefficient, respectively. Both $|S_{11}|$ and $|S_{21}|$ must be minimized at resonance frequency, f_r to achieve maximum absorption. Generally, the back surface of the absorber is fully covered by a metallic layer, and therefore the $|S_{21}| = 0$. In order to minimize the reflection, the air-absorber interface has to be impedance matched [8-9].

A. UNIT CELL DESIGN AND SIMULATION

The proposed metamaterial unit cell is a three-layered printed-circuit-board-based structure as illustrated in Figure 1. The substrate used is a flame retardant 4 (FR-4) with dielectric constant, $\varepsilon_r' = 4.3$; loss tangent, $\tan \delta = 0.025$; and thickness, $t_s = 1.6$ mm. This substrate is sandwiched between two copper layers (conductivity, $\sigma = 5.8 \times 10^7$ S/m; thickness of cooper, $t_c = 0.017$ mm). The copper layer at the back surface (ground layer) is fully covered to prohibit the transmission of microwave energy. Therefore, the $|S_{21}|$ is assumed to be negligible.
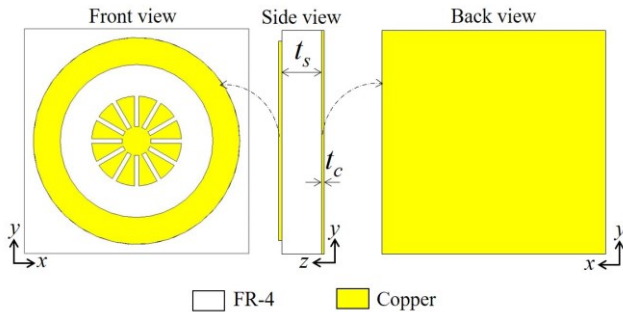

FIGURE 1. Three-layered metamaterial unit cell with resonator structure as the front layer and full metallic structure as the ground layer.

The copper layer at the front is the resonator structure. The front view of the unit cell structure is shown in Figure 2. The structure is designed to exhibit absorption at $f_r = 2.5$ GHz for the ring [refer to Figure 2 (a)] and $f_r = 5.8$ GHz for the circular patch with slits [refer to Figure 2 (b)]. As depicted in Figure 2 (c), the ring and circular patch with slits structures are combined within a same unit cell to form a hybrid structure, which exhibits dual-band absorption simultaneously at 2.5 GHz and 5.8 GHz.

The optimized dimensions of the ring structure [refer to Figure 2 (a)] consist of the inner diameter of ring, $d_1 = 17.0$ mm and width of cooper, $w = 3.0$ mm. The dimensions of the circular patch with slits [refer to Figure 2 (b)] are the diameter of circular patch, $d_2 = 10.0$ mm; width of slit, $a = 0.5$ mm; length of slit, $b = 3.4$ mm; and number of slits, $n = 12$. This resonator layer is designed to match with the characteristic impedance ($Z_o = 376.73$ Ω) of free space so that the $|S_{11}|$ is minimized at the resonance frequency, f_r.
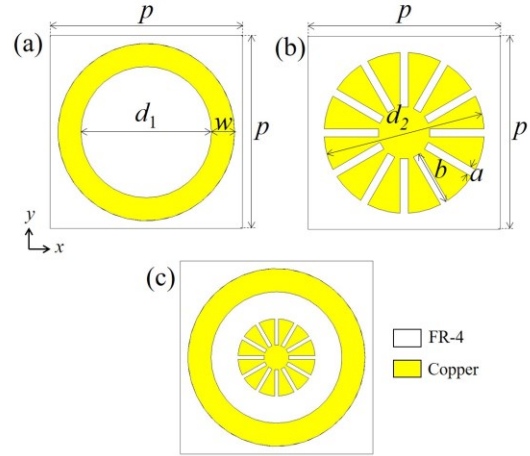

FIGURE 2. Front view of the metamaterial unit cell of a (a) ring; (b) circular patch with slits; (c) hybrid structure combining ring and circular patch with slits. ($a = 0.5$ mm, $b = 3.4$ mm, $d_1 = 17.0$ mm, $d_2 = 10.0$ mm, $p = 25.0$ mm, $w = 3.0$ mm)

The metamaterial unit cell is simulated using Computer Simulation Technology (CST) Microwave Studio. The unit cell structure is modelled as illustrated in Figure 3. The boundary conditions of the x-z and y-z planes are set as "Unit Cell" so that the modelled structure is repeated periodically in x-axis and y-axis directions up to infinity. A waveguide port is set to transmit the electromagnetic waves towards the unit cell structure and investigate the returning power. The absorptivity, α is calculated using Equation (1).
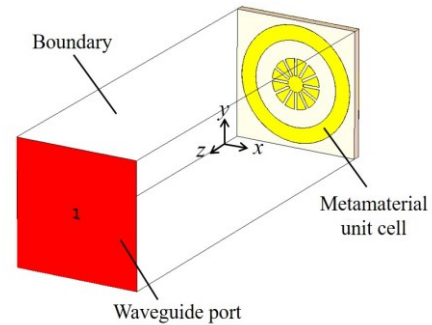

FIGURE 3. Simulation of metamaterial absorber unit cell.

B. PARAMETRIC STUDY AND OPTIMIZATION

An extensive parametric study is carried out to optimize and finalize the dimensions of the designed unit cell structure before the fabrication process. Figure 4 shows the absorptivity of the hybrid unit cell structure [refer to Figure 2 (c)] by varying the dimensions of the outer ring structure. Based on Figure 4 (a), the increment of the diameter of the

ring, d_1 shifts the absorption frequencies to lower frequencies. This is due to the increase in the electrical length of the ring structure when the diameter increases. When the electrical length increases, the ring structure supports standing waves of longer wavelength. Based on Figure 4 (b), when the width of ring, w increases, the absorption frequency is shifted to lower frequency.
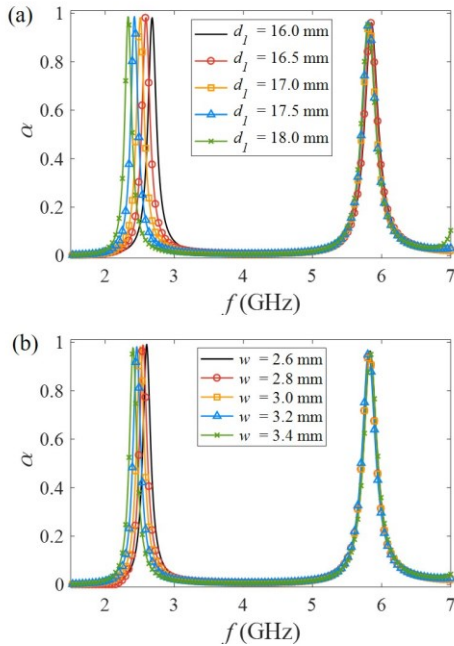

FIGURE 4. Absorptivity as a function of frequency of the hybrid unit cell structure for different value of (a) inner diameter of ring, d_1, (b) width of ring, w.

Figure 5 shows the absorptivity of the hybrid unit cell structure by varying the dimensions of the inner circular patch with slits structure. Based on Figure 5 (a), the increment of the diameter of the circular patch, d_2 will shift the resonance frequency to lower frequency. This is because the inner patch structure will resonate with the waves of longer wavelength when its size increases.

Based on Figure 5 (b), number of slits, n on the circular patch is investigated for $n = 4$ to $n = 12$ with a step of 2. When n increases, the absorption frequency shifts to higher frequency. Meanwhile, the overall magnitudes of absorptivity, α for various n are all higher than 0.95. This proves that n is a useful design parameter to tune the absorption performance of the proposed absorber to the desired frequency, without affecting the overall unit cell size, p.

The effects of the dimensions of slits (width of slit, a and length of slit, b) separating the circular sectors are provided in Figure 5 (c-d). Due to changes in capacitance, increases in both a and b shift the resonance frequency to lower frequency.

These parametric analyses are useful to investigate the effect of each geometrical parameter to the absorption performance of the absorbers. Furthermore, it serves as a reference for future absorber design processes at other desired operating frequencies. It can also be noticed that changing the dimension of the ring structure (refer to Figure 4) only shifts the resonance frequency of the first absorption peak, without significant effects on the frequency of the second absorption peak. Similarly, changing the dimensions of the circular patch with slits (refer to Figure 5) affects only the second absorption peak. This proves the design flexibility of the proposed absorber design using hybrid structures, in which both the absorption bands can be individually adjusted for other dual-band applications.
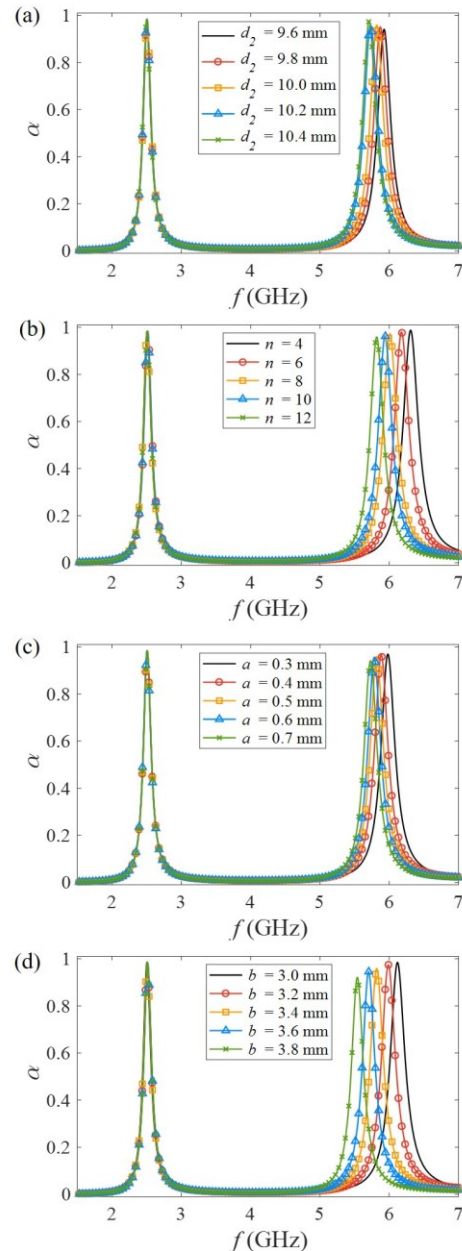

FIGURE 5. Absorptivity as a function of frequency of the hybrid unit cell structure for different value of (a) diameter of circular patch, d_2; (b) number of slits, n; (c) width of slit, a; (d) length of slit, b.

C. FABRICATION AND MEASUREMENT

A FR-4 substrate having a dimension of $200 \times 200 \times 1.6$ mm^3 is used for the prototype fabrication. As illustrated in Figure 6, an array of 7×7 unit cells is printed on the substrate using conventional printed circuit board (PCB) fabrication technique.
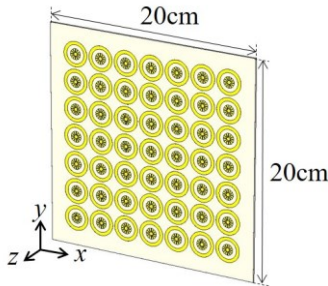

FIGURE 6. Illustration of the prototype metamaterial absorber consists of 7 × 7 array of hybrid unit cell structures combining rings and circular patches with slits printed on a FR-4 substrate.

The free-space measurement experimental setup as described in [10-11] is illustrated in Figure 7. A wideband directional antenna, which is connected to an E5071C vector network analyzer manufactured by Keysight Technologies, is used to transmit the electromagnetic energy towards the proposed metamaterial absorber and receive the reflected energy.
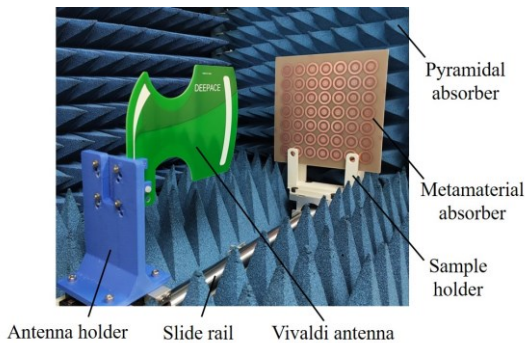

FIGURE 7. Experimental setup of free-space measurement for metamaterial absorber.

III. RESULTS AND DISCUSSION

In this section, the absorption performance of the proposed metamaterial absorber is discussed. Furthermore, the application of the proposed absorber as a sensing structure for the determination of the dielectric constant of materials is presented.

A. ABSORPTION PERFORMANCE

Figure 8 shows the magnitude of the reflection coefficient, $|S_{11}|$ of the proposed metamaterial absorbers. Based on the experimental results, the ring-based absorber [refer to Figure 8 (a)] exhibits resonance at $f_r = 2.5$ GHz whereas the circular-patch-based absorber [refer to Figure 8 (b)] exhibits resonance at $f_r = 6.0$ GHz. When these two structures are

combined within a same unit cell to form the hybrid absorber, the absorber resonates at both resonance frequencies as shown in Figure 8 (c). It is worth mentioning that this design approach is effective for a dual-band absorber, as the resulting f_r does not shift slightly to other frequencies when both structures are combined within the same unit cell. Furthermore, all the $|S_{11}|$ at resonance frequencies are better than -15 dB.

With reference to the simulated results, the hybrid absorber is designed to resonate at $f_r = 2.5$ GHz and $f_r = 5.8$ GHz. The experimentally measured f_r agrees with the simulated f_r for the first resonance at $f_r = 2.5$ GHz. However, for the second resonance, the measured f_r shifted to 6.0 GHz. This discrepancy between the simulated and measured f_r is caused by fabrication errors as the circular patch structure contains slit structures with small dimensions.
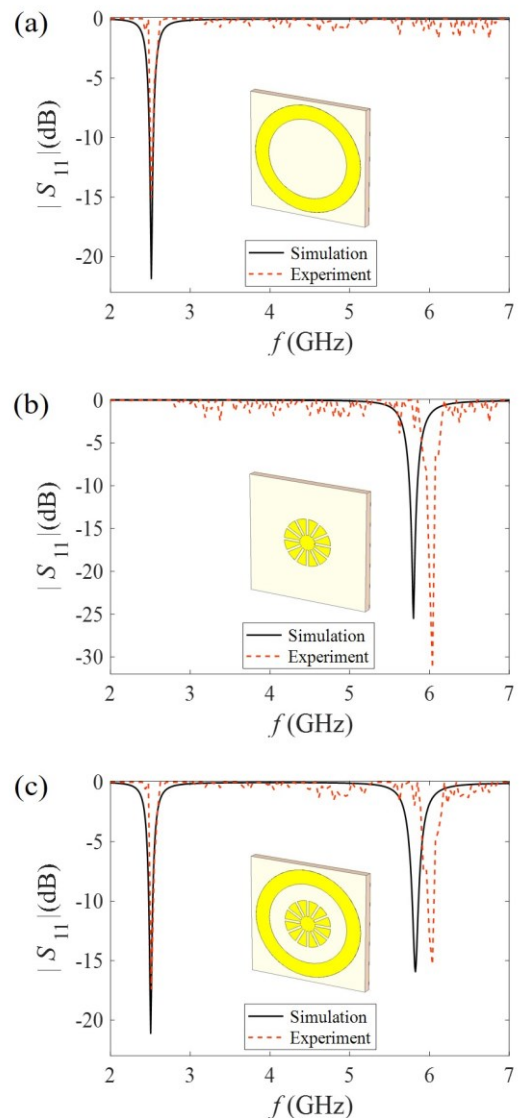

FIGURE 8. Simulated and measured reflection coefficient, |S$_{11}$| of the metamaterial absorber array based on (a) rings, (b) circular patches with slits, (c) hybrid structures

Figure 9 shows the experimentally measured absorptivity, α of the fabricated metamaterial absorber prototype. It can be seen that all the absorptivity, α at the resonance frequencies are near-unity ($\alpha > 0.97$). This shows that the proposed absorbers are able to absorb more than 97% of the incoming microwave power at both resonance frequencies.
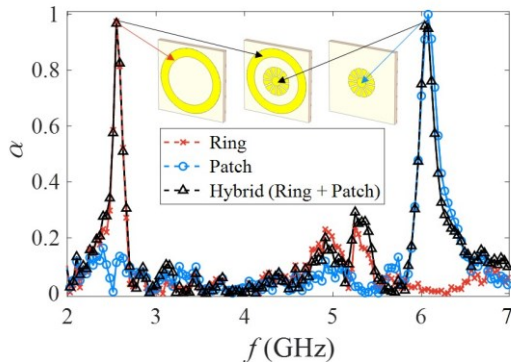

FIGURE 9. Measured absorptivity, α of the proposed metamaterial absorbers.

The absorption performance of the proposed dual-band absorber under different angles of incidence, θ is shown in Figure 10. Based on Figure 10 (b), the magnitude of the maximum absorptivity, α approaches unity value for $\theta = 0º$, 15º, 30º, and 45º at the resonance frequencies. However, the maximum α at the resonance frequencies diminished for $\theta = 60º$ and 75º. The relationship between the maximum α and θ is shown in Figure 10 (c). The absorber is able to maintain >80% absorption ($\alpha > 0.8$) for both absorption bands up to $\theta = 55º$. This shows that the proposed absorber can operate at considerably wide angle of incidence.

The absorption performance of the absorber under different angles of polarization, ϕ is shown in Figure 11. The absorptivity, α remains almost unchanged at both resonance frequencies under different ϕ. This result is as expected based on the symmetrical design of the proposed absorber. The rotational symmetry order of the circular patch with slits structure is as high as 12, which means that the structure is geometrically similar with respect to different ϕ. This shows that the proposed absorber is polarization insensitive.

The incident electromagnetic waves interact with the geometrical features of the metallic conductor, especially the discontinuities or sharp edges [12]. This results in the induction of fringing fields in particular regions of the resonant structure and contributes to the formation of localized resonances. Figure 12 shows the electric, E and magnetic, H field distributions at resonance frequencies f_r. At $f_r = 2.5$ GHz, the electric field, E, is concentrated at both vertical sides of the ring whereas magnetic field, H, is concentrated at both horizontal sides of the ring. This is due to the standing waves that are set up on the ring structure during the resonance [11]. At $f_r = 5.8$ GHz, the electric field, E is concentrated at both vertical sides of the circular patch. The magnetic field, H is concentrated mostly at the slits near

the inner part of the patch. The slits with appropriate sizes are strategically placed to tailor the impedance for impedance matching.
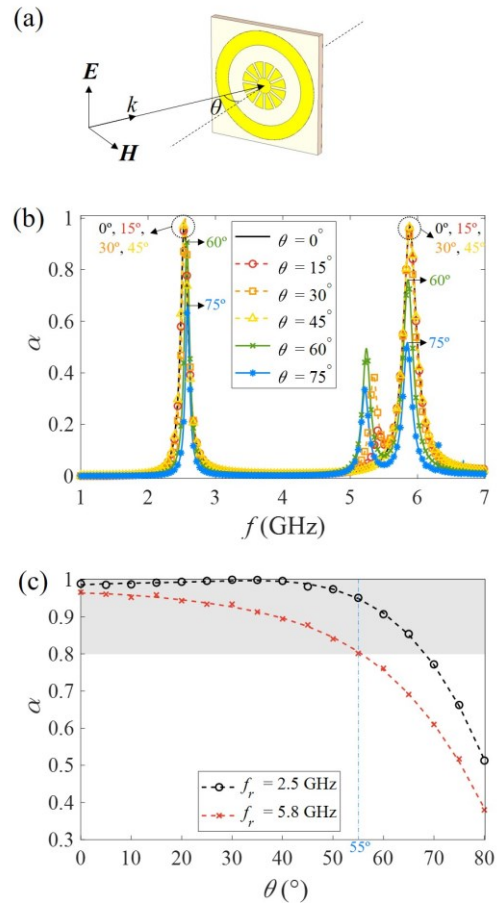

FIGURE 10. (a) Hybrid absorber under oblique angle of incidence, θ, and its (b) plot of absorptivity against frequency for different θ, and (c) plot of maximum absorptivity against θ at both resonance frequencies, f_r (grey region indicates $\alpha > 0.8$).
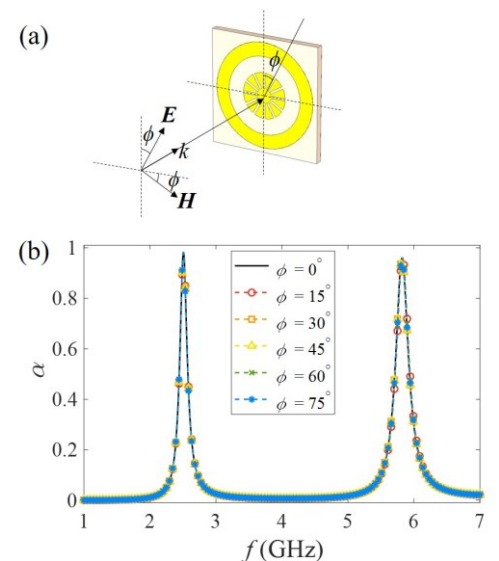

FIGURE 11. (a) Hybrid absorber under oblique angle of polarization, ϕ, and its (b) plot of absorptivity against frequency for different ϕ.
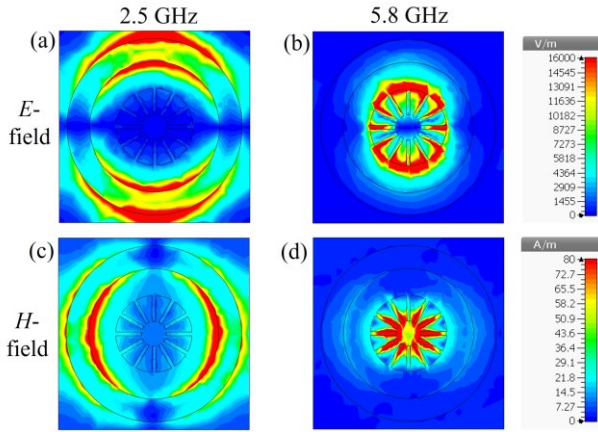
FIGURE 12. Electric field distribution at (a) 2.5 GHz, and (b) 5.8 GHz; Magnetic field distribution at (c) 2.5 GHz, and (d) 5.8 GHz of the proposed ring-patch hybrid absorber

The high magnetic resonance responses can be explained using the anti-parallel current theory [13-14]. The surface current, I distributions at both resonance frequencies are illustrated in Figure 13. At f_r = 2.5 GHz, the direction of current flow in the upper ring structure and the ground surface is in the opposite direction. Similarly, at f_r = 5.8 GHz, the current flow in the circular patch is in the opposite direction to the current flow in the ground. These anti-parallel surface currents enable the excitations of the magnetic dipoles and occurrence of magnetic resonances.
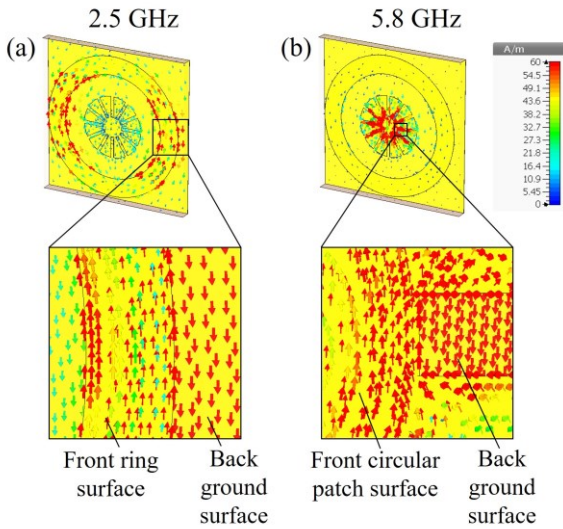

FIGURE 13. Surface current distribution on the copper surfaces at (a) 2.5 GHz, and (b) 5.8 GHz

To extract the equivalent electromagnetic properties, the proposed absorber is quantitatively analyzed using the symmetry model method [15-17]. As shown in Figure 14, the new symmetrical structure, which consists of two unit cells arranged back-to-back in mirror symmetry, are constructed without the metal plate. The S-parameters (S_{11} and S_{21}) of this composite medium are obtained from CST simulation.
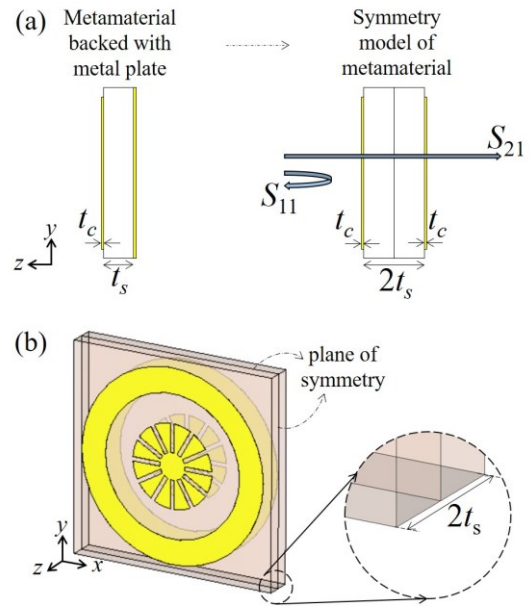

FIGURE 14. (a) Schematic side view of the construction of symmetry model for metamaterial having a total thickness of $t_{total} = 2(t_s+t_c)$, (b) Perspective view of the constructed symmetry model for the proposed absorber.

The normalized impedance, Z of the metamaterial symmetry model can be expressed as [18]:

$$Z = \sqrt{\frac{(1+S_{11})^2 - S_{21}^2}{(1-S_{11})^2 - S_{21}^2}} \qquad (2)$$

where S_{11} and S_{21} are complex reflection coefficient and complex transmission coefficient, respectively.

The refractive index, n can be determined as:

$$n = \frac{1}{kt_{total}}\cos^{-1}\left[\frac{1}{2S_{21}}\left(1 - S_{11}^2 + S_{21}^2\right)\right] \qquad (3)$$

where $t_{total} = 2(t_s+t_c)$ = 3.234 mm is the total thickness of the symmetry model, and k is the wave number of the incident wave in free space.

Using Z and n from (2) and (3), the relative complex permittivity, ε_r ($= \varepsilon_r' - j\varepsilon_r''$) and relative complex permeability, μ_r ($= \mu_r' - j\mu_r''$) of the composite medium can be calculated as:

$$\varepsilon_r = \frac{n}{Z} \qquad (4)$$

$$\mu_r = nZ \qquad (5)$$

The extracted ε_r and μ_r are shown in Figure 15. Based on Figure 15 (b), the real part of relative permeability, μ_r' of the metamaterial composite medium exhibits two significant peaks at f = 2.5 GHz and f = 5.8 GHz, in which the μ_r' achieves 6.7 and 2.0 at both peaks, respectively, while maintaining close to 1 for other frequency range. The sharp

increment of μ_r' at both frequencies indicates magnetic resonance. This is known as true magnetic resonance, in which the current wave travels around the resonator structure constructively and builds up to a large quantity [19-20]. The value of μ_r' is negative at the frequency ranges of 2.51 GHz to 3.11 GHz and 5.95 GHz to 6.37 GHz.

The magnetic resonant response in μ_r is accompanied by simultaneous anti-resonant behavior in ε_r [21]. With reference to Figure 15 (a), the imaginary part of relative permittivity, ε_r'' becomes negative, and the real part of relative permittivity, ε_r' shows "reversed" Lorentz-shaped curve in the vicinity of magnetic resonance [22]. This unusual non-Lorentzian behavior is associated with spatial dispersion in periodic structures [22].
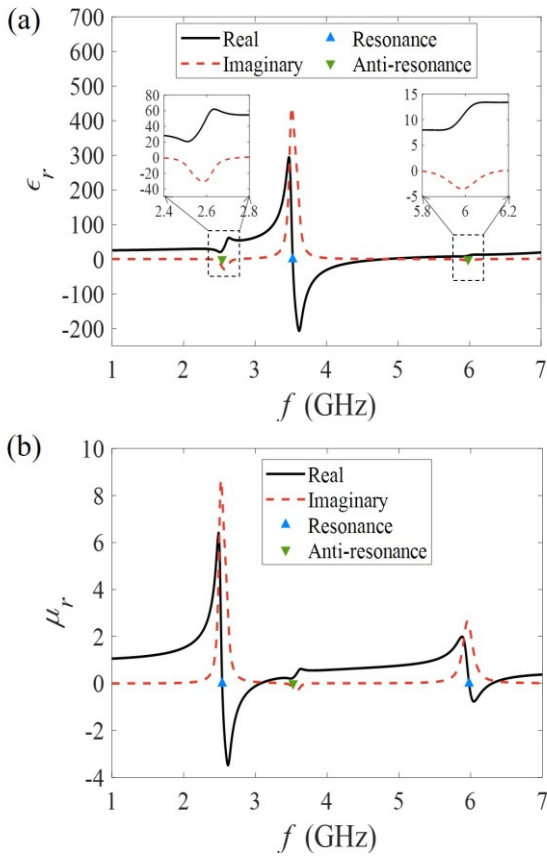

FIGURE 15. Extracted equivalent (a) relative complex permittivity (b) relative complex permeability of the metamaterial symmetry model.

The extracted ε_r and μ_r can be used with the transmission line theory to determine the magnitude of the reflection coefficient, $|S_{11}|$ of the metamaterial absorber backed by metal plate (refer to Figure 3). The input impedance, Z_{in} of the metamaterial absorber backed by metal plate can be expressed as [15]:

$$Z_{in} = Z_o \sqrt{\frac{\mu_r}{\varepsilon_r}} \tanh\left[j\left(\frac{2\pi f \left(t_s + t_c\right)}{c} \right) \sqrt{\mu_r \varepsilon_r} \right] \quad (6)$$

where c is the velocity of electromagnetic waves in free space, f is the frequency of the incident microwave, Z_o is the characteristic impedance of free space, and j is the imaginary constant.

Finally, the magnitude of the reflection coefficient, $|S_{11}|$ (in dB) of the absorber can be calculated as:

$$\left|S_{11}\right|(\text{dB}) = 10 \log \left| \frac{Z_{in} - Z_o}{Z_{in} + Z_o} \right| \quad (7)$$

Figure 16 (a) shows the Z_{in} of the metamaterial absorber as a function of frequency. At the resonance frequencies, the imaginary part of the input impedance goes to zero [23]. This implies that the structure is purely resistive and it dissipates energy. The real part of the input impedance is also close to the characteristic impedance of free space, leading to minimal reflection. Therefore, absorption occurs at the resonance frequencies. Based on Figure 16 (b), the $|S_{11}|$ of the metamaterial absorber determined by the theoretical model is consistent with the simulated $|S_{11}|$ using CST.
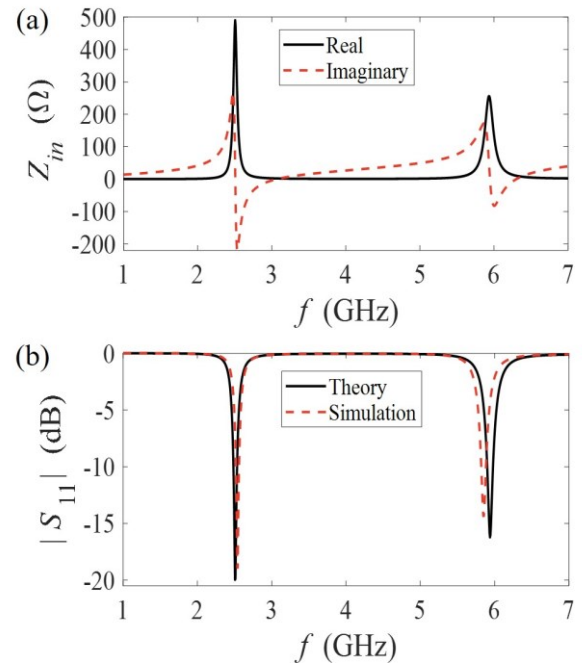

FIGURE 16. (a) Input impedance, Z_{in} of the metamaterial absorber, (b) Comparison of reflection coefficient, $|S_{11}|$ of the metamaterial absorber determined using theoretical calculation (based on symmetry model theory) and numerical simulation (using CST).

B. SENSING APPLICATION

The enhanced concentrated field and narrow bandwidth characteristics of metamaterials are desired for sensing applications. The proposed absorber is demonstrated in the determination of dielectric constant, ε_r' for thin flat planar dielectric samples using the first resonance peak at $f_r = 2.5$ GHz. The operating principle of the absorber as a dielectric sensor is based on the shift in the resonance frequency, Δf_r, which is the difference between the f_r of the unloaded

metamaterial and f_r of the metamaterial loaded with sample under test (SUT). Different value of $\varepsilon_{r'}$ will shift the resonance frequency, f_r to a different extent. By measuring Δf_r, the value of $\varepsilon_{r'}$ can be estimated.

The absorber is loaded with SUTs having thickness of t by placing them in close proximity with the absorber structure as illustrated in Figure 17. To obtain the relationship between the $\varepsilon_{r'}$ of the SUT and the f_r, the absorber loaded with SUT having different $\varepsilon_{r'}$ and t are simulated. The simulation result is shown in Figure 18. The Δf_r is dependent on the $\varepsilon_{r'}$ and t of the SUT.
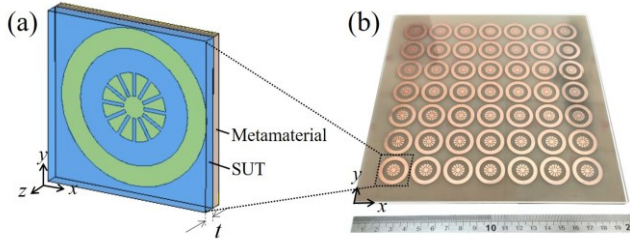

FIGURE 17. Metamaterial absorber loaded with a thin flat planar dielectric SUT having thickness of t: (a) Unit cell, (b) Array.
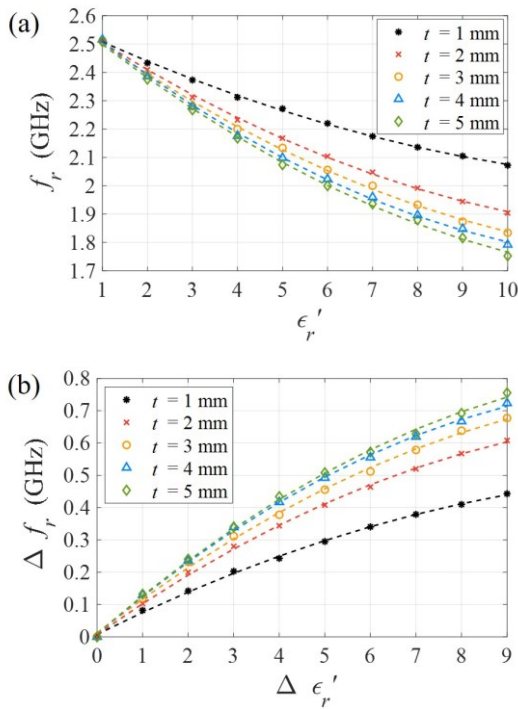

FIGURE 18. Simulated (a) resonance frequency, f_r against the dielectric constant, $\varepsilon_{r'}$ for different thicknesses, t of the SUT, (b) shift of resonance frequency, Δf_r against change in dielectric constant, $\Delta\varepsilon_{r'}$ of the SUT.

Through polynomial fitting, $\varepsilon_{r'}$ can be estimated from the measured Δf_r (in GHz) and t (in mm) using equation (8) as:

$$\varepsilon_r' = (-0.67t^3 + 7.42t^2 - 27.01t + 41.56)\Delta f_r^2 + ...$$
$$(-0.11t^3 + 1.42t^2 - 6.39t + 15.70)\Delta f_r + 1. \quad (8)$$

Equation (8) is valid for $\varepsilon_{r'}$ and t ranges up to 10 and 5 mm, respectively.

For validation purpose, four dielectric SUTs, which are Teflon, acrylic, nylon, and FR-4 are investigated experimentally. The thicknesses, t of the SUTs are measured using a digital Vernier calliper. The $\varepsilon_{r'}$ of the SUTs are measured using a dielectric probe aided with Filpal dielectric measurement software and Fieldfox N9925A network analyzer manufactured by Keysight Technologies, as shown in Figure 19 (a) [24]. The measured values of $\varepsilon_{r'}$ are shown in Figure 19 (b). The measured typical value of $\varepsilon_{r'}$ of Teflon, acrylic, nylon, and FR4 are 2.06, 2.82, 3.20, and 4.36, respectively.
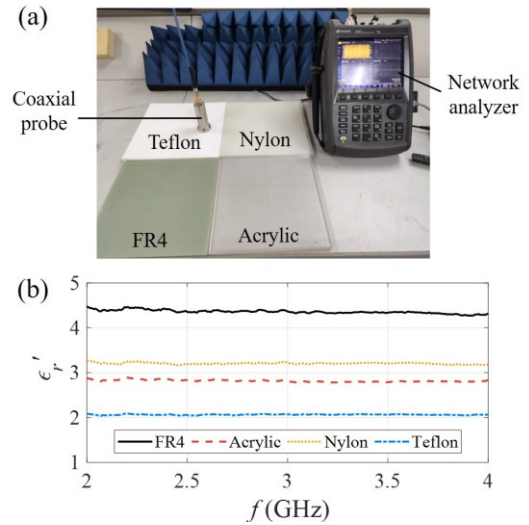

FIGURE 19. (a) Experimental measurement using coaxial probe, (b) Measured dielectric constant for the SUTs.

The resonance frequency, f_r of the absorber loaded with SUTs are then measured using the same aforementioned free-space experimental setup (refer to Figure 7). Δf_r is determined from the difference of f_r for metamaterial loaded with SUT and f_r for unloaded metamaterial, which is 2.51 GHz. The measured Δf_r and t are substituted into equation (8) to calculate $\varepsilon_{r'}$. These predicted $\varepsilon_{r'}$ are tabulated in Table I.

Based on Table I, the predicted $\varepsilon_{r'}$ for the SUTs are in considerable agreement with the measured $\varepsilon_{r'}$ using dielectric probe. The discrepancies are mainly due to the errors that have arisen from the Δf_r measurement. This includes the air gap between the absorber and the SUT, as the SUTs do not have an entirely flat surface. For SUTs with a low value of $\varepsilon_{r'}$, the predicted $\varepsilon_{r'}$ might vary more significantly due to the fact that small changes in Δf_r will lead to a bigger variation in the $\varepsilon_{r'}$ [refer to Figure 18 (b)).

Despite the errors, the functionality of the proposed absorber is still competent. The sensors can be used to compare SUTs with slight differences in $\varepsilon_{r'}$ value. This is particularly useful in applications such as defect detection, adulteration detection, and concentration determination.

TABLE I. Comparison of dielectric constant, ε_r' of SUTs measured using probe, and predicted using Equation (8).

SUT	t (mm)	Measured f_r (GHz)	Measured ε_r'	Predicted ε_r'	Relative errors, $|\Delta \varepsilon_r' / \varepsilon_r'| \times 100$ (%)
Teflon	2.01	2.42	2.06	1.79	13.1
Acrylic	1.70	2.36	2.82	2.57	8.9
Nylon	2.08	2.30	3.20	3.09	3.4
FR4	2.07	2.21	4.36	4.31	0.2

IV. CONCLUSION

A wide-angle polarization-insensitive dual-band microwave absorber operating at 2.5 GHz and 5.8 GHz simultaneously is proposed using ring and circular patch with slits structures. The design is simple, and each absorption band can be individually adjusted. Furthermore, the absorber can be applied in sensing applications to estimate the dielectric constants of thin planar dielectric samples.

ACKNOWLEDGMENT

REFERENCES

[1] B. X. Wang, C. Xu, G. Duan, W. Xu, and F. Pi, "Review of broadband metamaterial absorbers: from principles, design strategies, and tunable properties to functional applications," *Advanced Functional Materials*, vol. 33, no. 14, pp. 2213818, 2023, DOI: 10.1002/adfm.202213818.

[2] P. Jain, A. K. Singh, J. K. Pandey, S. Garg, S. Bansal, M. Agarwal, S. Kumar, N. Sardana, N. Gupta, and A. K. Singh, "Ultra-thin metamaterial perfect absorbers for single-/dual-/multi-band microwave applications." *IET Microwaves, Antennas & Propagation*, vol. 14, no. 5, pp. 390-396, 2020, DOI: 10.1049/iet-map.2019.0623.

[3] M. Berka, U. Özkaya, T. Islam, M. El Ghzaoui, S. Varakumari, S. Das, and Z. Mahdjoub, "A miniaturized folded square split ring resonator cell based dual band polarization insensitive metamaterial absorber for C-and Ku-band applications," *Optical and Quantum Electronics*, vol. 55, no. 8, pp. 699, 2023, DOI: 10.1007/s11082-023-04954-y.

[4] A. X. Wang, S. B. Qu, M. B. Yan, W. J. Wang, J. F. Wang, L. Zheng, and J. L. Wang, "Six-band polarization-insensitive perfect metamaterial absorber using L-shaped resonators," *Applied Physics A*, vol. 125, pp. 331, 2019, DOI: 10.1007/s00339-019-2568-y.

[5] Q. Huang, G. Wang, M. Zhou, J. Zheng, S. Tang, and G. Ji, "Metamaterial electromagnetic wave absorbers and devices: Design and 3D microarchitecture," *Journal of Materials Science & Technology*, vol. 108, pp. 90-101, 2022, DOI: 10.1016/j.jmst.2021.07.055.

[6] K. S. L. Al-badri, Y. I. Abdulkarim, F. Ö. Alkurt, and M. Karaaslan, "Simulated and experimental verification of the microwave dual-band metamaterial perfect absorber based on square patch with a 45º diagonal slot structure," *Journal of Electromagnetic Waves and Applications*, vol. 35, no. 11, pp. 1541-1552, 2021, DOI: 10.1080/09205071.2021.1905560.

[7] S. Fang, L. Deng, P. Zhang, L. Qiu, H. Xie, J. Du, H. Wang, and H. Zhao, "Dual-band metamaterial absorber with stable absorption performance based on fractal structure," *Journal of Physics D: Applied Physics*, vol. 55, no. 9, pp. 095003, 2021, DOI: 10.1088/1361-6463/ac3864.

[8] G. Duan, J. Schalch, X. Zhao, A. Li, C. Chen, R. D. Averitt, and X. Zhang, "A survey of theoretical models for terahertz electromagnetic metamaterial absorbers," *Sensors and Actuators A: Physical*, vol. 287, pp. 21-28, 2019, DOI: 10.1016/j.sna.2018.12.039.

[9] J. Wen, Y. Wang, and Y. Wang, "Advanced Engineering Design of the Metamaterial Absorbers," in *Metamaterial Technology and Intelligent Metasurfaces for Wireless Communication Systems*, Hershey, PA, USA: IGI Global, 2023, ch.7, pp. 136-179. [Online] Available: https://www.igi-global.com/book/metamaterial-technology-intelligent-metasurfaces-wireless/312573

[10] K. Y. You, M. S. Sim, H. Mutadza, F. Esa, and Y. L. Chan, "Free-space measurement using explicit, reference-plane and thickness-invariant method for permittivity determination of planar materials," in *2017 Progress in Electromagnetics Research Symposium-Fall (PIERS-FALL)*, Singapore, 2017, pp. 222-228.

[11] M. S. Sim, K. Y. You, F. Esa, M. N. Dimon, and N. H. Khamis, "Multiband metamaterial microwave absorbers using split ring and multiwidth slot structure," *International Journal of RF and Microwave Computer-Aided Engineering*, vol. 28, no. 7, pp. e21473, 2018, DOI: 10.1002/mmce.21473.

[12] C. A. Valagiannopoulos, "On smoothening the singular field developed in the vicinity of metallic edges," *International Journal of Applied Electromagnetics and Mechanics*, vol. 31, no. 2, pp. 67-77, 2009, DOI: 10.3233/JAE-2009-1048.

[13] J. Zhou, E. N. Economon, T. Koschny, and C. M. Soukoulis, "Unifying approach to left-handed material design," *Optics letters*, vol. 31, no. 24, pp. 3620-3622, 2006, DOI: 10.1364/OL.31.003620.

[14] L. Stephen, N. Yogesh, and V. Subramanian, "Realization of bidirectional, bandwidth-enhanced metamaterial absorber for microwave applications," *Scientific Reports*, vol. 9, no. 1, pp. 10058, 2019, DOI: 10.1038/s41598-019-46464-6.

[15] H. Xiong, Q. Yang, Z. C. Huang, W. X. Peng, and H. Q. Zhang, "Analyzing broadband tunable metamaterial absorbers by using the symmetry model," *Optics Express*, vol. 29, no. 25, pp. 41475-41484, 2021, DOI: 10.1364/OE.442115.

[16] J. Zhang, D. He, G. Wang, P. Wang, L. Qiao, T. Wang, and F. Li, "Equivalent electromagnetic parameters for microwave metamaterial absorber using a new symmetry model," *Chinese Physics B*, vol. 28, no. 5, pp. 058401, 2019, DOI: 10.1088/1674-1056/28/5/058401.

[17] C. A. Valagiannopoulos and S. A. Tretyakov, "Symmetric absorbers realized as gratings of PEC cylinders covered by ordinary dielectrics," *IEEE Transactions on Antennas and Propagation*, vol. 62, no. 10, pp. 5089-5098, 2014, DOI: 10.1109/TAP.2014.2340891.

[18] D. R. Smith, D. C. Vier, T. Koschny, and C. M. Soukoulis, "Electromagnetic parameter retrieval from inhomogeneous metamaterials," *Physical review E*, vol. 71, no. 3, pp. 036617, 2005, DOI: 10.1103/PhysRevE.71.036617.

[19] A. F. McKinley, T. P. White, I. S. Maksymov, and K. R. Catchpole, "The analytical basis for the resonances and anti-resonances of loop antennas and meta-material ring resonators," *Journal of Applied Physics*, vol. 112, no. 9, pp. 094911, 2012, DOI: 10.1063/1.4764104.

[20] T. Koschny, P. Markoš, D. R. Smith, and C. M. Soukoulis, "Resonant and antiresonant frequency dependence of the effective parameters of metamaterials," *Physical Review E*, vol. 68, no. 6, pp. 065602, 2003, DOI: 10.1103/PhysRevE.68.065602.

[21] X. Gao, F. L. Yu, C. L. Cai, C. Y. Guan, J. H. Shi, and F. Hu, "Terahertz metamaterial with broadband and low-dispersion high refractive index," *Optics Letters*, vol. 45, no. 17, pp. 4754-4757, 2020, DOI: 10.1364/OL.397230.

[22] Y. A. Urzhumov, G. Shvets, J. Fan, F. Capasso, D. Brandl, and P. Nordlander, "Plasmonic nanoclusters: a path towards negative-index metafluids," *Optics express*, vol. 15, no. 21, pp. 14129-14145, 2007, DOI: 10.1364/OE.15.014129.

[23] K. Y. You, "Analytical modeling of bare monopole driven from coaxial line," in *RF coaxial slot radiators: Modeling, measurements, and applications*, London, England: Artech House, 2016, pp. 57-89.

[24] K. Y. You and M. S. Sim, "Precision permittivity measurement for low-loss thin planar materials using large coaxial probe from 1 to 400 MHz," *Journal of Manufacturing and Materials Processing*, vol. 2, no. 4, pp. 81, 2018, DOI: 10.3390/jmmp2040081.